

# Confocal microscopy of geometrically frustrated hard sphere crystals

Roel P.A. Dullens<sup>1,2</sup>, Volkert W.A. de Villeneuve<sup>1</sup>, Maurice C.D. Mourad<sup>1</sup>, A.V. Petukhov<sup>1</sup> and Willem K. Kegel<sup>1</sup>

<sup>1</sup> Van 't Hoff Laboratory for Physical and Colloid Chemistry, Debye Institute, Utrecht University, Padualaan 8, 3584 CH Utrecht, The Netherlands

<sup>2</sup> 2. Physikalisches Institut, Universität Stuttgart, 70569 Stuttgart, Germany

Received: date / Revised version: date

**Abstract.** Confocal microscopy has been used to study the crystallization of two colloidal model systems that are geometrically frustrated in a completely different way: (I) hard colloidal polyhedrals, where crystallization is frustrated due to the incommensurate particle shape and (II) large spherical impurities in a sea of monodisperse colloidal hard spheres, where crystallization is frustrated by the introduction of impurities. As a reference system, we analyzed the crystallization of pure monodisperse colloidal hard spheres. We show that although the crystal structures of both systems are highly dissimilar on the individual particle level, both sources of geometrical frustration have a similar effect on the structure on the grain level. We quantitatively characterize the polycrystalline structures and study the crystallization process in time. Whereas grain boundaries persist in the frustrated systems due to structural arrest, the majority of grain boundaries anneals out quite rapidly in the reference system. Therefore, we argue that both sources of geometrical frustration cause a polycrystalline structure.

**PACS.** 61.72 Mn Grain and twin boundaries – 61.82 Rx Nanocrystalline materials – 82.70 Dd Colloids

## 1 Introduction

Crystals are characterized by perfect periodic order. However, in practice crystals always exhibit various types of imperfections or defects such as vacancies, dislocations, stacking faults, grain boundaries and impurities [1]. Defects can arise since these are frozen in during crystal growth or formed due to stress on the crystal. Furthermore, they strongly influence macroscopic properties of many materials like semiconductors, metals and ceramics [2]. Grain boundaries in crystals crucially influence the mechanical properties, as the grain size is directly related to the strength of materials [1–4]. For relatively small grain sizes the strength increases with increasing grain size [4–6], while for larger grain sizes the materials strengthens if the crystallites gets smaller (Hall-Petch effect) [7, 8]. Therefore, controlling the grain size, for instance by tuning the solidification rate, heating or mechanical annealing, is of paramount importance in material science [1, 3, 9, 10].

Studying grain boundary formation and grain growth in atomic and molecular crystals in real-space is rather difficult due to the small length scales involved in atomic and molecular systems. Consequently, computer simulations have proven to be beneficial to study these issues on the atomic level [11–17]. Inherent to their typical size, colloidal systems provide an excellent tool to address these issues experimentally. In contrast to atomic systems, col-

loidal systems consist of particles with a characteristic size between a nanometer and several micrometers. This length scale makes them very suitable to be studied in real-space and real-time by microscopy techniques [18–20]. In particular, the combination of advanced colloidal particles and confocal microscopy has already made it possible to study several fundamental condensed matter problems, such as freezing, melting and glass formation, on the single-particle level [10, 18–32]. Interestingly, colloidal systems exhibit similar phase-behaviour as atomic systems, making colloids a powerful model-system for condensed matter and atomic materials [33–36].

In this work, we consider two colloidal model systems that exhibit completely different types of geometrical frustration: the crystals of the colloidal polyhedrals are frustrated due to incommensurate particle shape [37], whereas the crystals in the second system are frustrated by the addition of model impurities [28, 30]. The influence of particle shape is e.g. relevant for applications in powder technology and ceramics [38], while the colloidal crystal containing impurities may serve as a model system for nanocrystalline materials containing dopants [15–17, 39]. In our previous work we studied the structure of single crystalline domains of hard polyhedral colloids, without considering grain boundaries [37]. Furthermore, we addressed the influence of the presence of impurities on the dynamics of crystallization of colloidal hard spheres, without quantita-

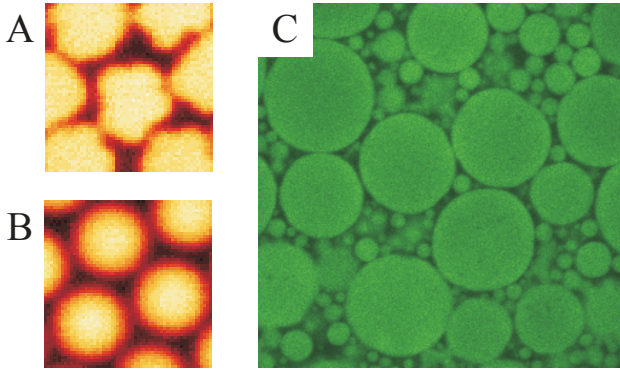


**Fig. 1.** Confocal microscopy images of (A) the polyhedral particles and (B) the spherical reference particles ( $9 \times 9 \mu\text{m}^2$ ). (C) Confocal image of the impurities ( $70 \times 70 \mu\text{m}^2$ ) directly after synthesis. The larger particles (i.e.  $d_i \in 7.5 - 31.5 \mu\text{m}$ ) were used as model impurities in a sea of small monodisperse particles ( $d_p = 1.5 \mu\text{m}$ ).

tively analyzing the final crystal structure [28,30]. Here, we use real-space confocal microscopy [40] to quantitatively characterize the polycrystalline structure of geometrically frustrated colloidal crystals. Our results clearly show that both sources of geometrical frustration—which are completely different in nature—significantly reduce the grain size of the colloidal crystals in a very similar way. In addition, we investigate the arrested grain growth by identifying the (time-dependent) defect-structure during grain growth.

## 2 Experimental

The ‘*polyhedral system*’ consists of crosslinked and fluorescently labeled polymethyl methacrylate (PMMA) colloids that are monodisperse in size, but exhibit a polyhedral particle shape [37,41] (see Fig. 1 A). In our experiments, we compare the polyhedrals to a reference system of spherical and size-monodisperse reference PMMA particles of equal size [42] (see Fig. 1B). The diameters  $d$  of the polyhedral and reference particles are respectively  $d = 2.23 \pm 0.09$  and  $d = 2.33 \pm 0.07$ . The ‘*impurity system*’ consists of a sea of fluorescently labeled monodisperse PMMA particles with a diameter  $d_p$  of  $1.5 \pm 0.09 \mu\text{m}$  containing a small fraction of very large PMMA particles, called the impurities [28,30]. The impurities were obtained by a synthesis following [42]. The resulting particles were extremely polydisperse and very large ( $d_i \in 0.1 - 100 \mu\text{m}$ ) as illustrated in Fig. 1C. Impurities of different sizes were separated by repeated sedimentation. Subsequently a small amount (typically  $< 0.1$  weight %) of impurities of the desired size was added to a sea of small PMMA particles. As a result, systems of monodisperse PMMA spheres contaminated with differently sized model impurities were obtained. Obviously, the reference system is formed by the same monodisperse PMMA spheres ( $d_p = 1.5 \mu\text{m}$ ) without impurities. The impurity systems are characterized by the size ratio between the particles and the impurities

$\alpha \equiv (d_i/d_p)m$  with  $d_i$  and  $d_p$  respectively the diameters of the impurity and the particles. In this work, we consider impurity systems with  $\alpha = 5, 8, 13$  and  $21$ .

The colloidal model systems were dispersed in a mixture of cis-decalin (Merck, for synthesis), tetralin (Merck, for synthesis) and carbontetrachloride (Merck, for spectroscopy), which simultaneously matches the refractive index and almost the mass density of the particles [30,43]. In this solvent the particles interact via a hard-sphere-like potential [43,44]. The dispersions were contained in small homemade vials [43] and the particles were imaged using a Nikon TE 2000U inverted microscope with a Nikon C1 confocal scanning laser head. For the polyhedral colloids, samples with a volume fraction  $\phi \equiv \rho v \approx 0.40$  were prepared (with  $\rho$  the number density and  $v$  the particle’s volume). The impurity systems were prepared at relatively high volume fraction ( $\phi \approx 0.55$ ) to minimize the mobility of the impurity during the measurements [28,30]. The volume fractions of the samples were defined relative to the random close packing density at the relevant polydispersity [45].

In the polyhedral, the impurity and the reference systems the colloidal crystal heterogeneously nucleates at the wall, followed by subsequent upward growth [28,30,32,46]. As a result, the (111)-plane of the crystal is oriented at the wall, allowing a quantitative 2D in-plane analysis of the systems [24,28,30,37,46,47]. The structure of the polyhedrals was analyzed after slow sedimentation had fully completed as the influence of the particle shape is most pronounced at highest compression. Since the layering in the polyhedral system did not persist in bulk [37], we studied the first layer at the glass wall in this system. Although certainly interesting, the question as to how the structure of the polyhedrals evolves in the third dimension lies outside the scope of this work. The impurity system was studied in the plane corresponding to the center of the impurity, which was typically  $20 \mu\text{m}$  above the glass wall. Furthermore, we studied the time-dependent structure of both systems during crystallization. The centers of the particles were located using image-analysis software similar to that described in [48]. We verified that the polyhedral particle shape did not significantly affect the accuracy of the particle tracking.

## 3 Results and discussion

Representative confocal micrographs of the colloidal crystal formed by the frustrated and reference systems are shown in Fig. 2. The structure of both the polyhedrals and the impurity system exhibit a much higher degree of polycrystallinity compared to the structure formed by the reference spheres. To quantify this, we computed the radial distribution function  $g(r)$  (being proportional to the probability of observing a particle a distance  $r$  away from a given particle):

$$g(r) = \frac{1}{\rho} \left\langle \sum_{j \neq i} \delta(r_i - r_j - r) \right\rangle. \quad (1)$$

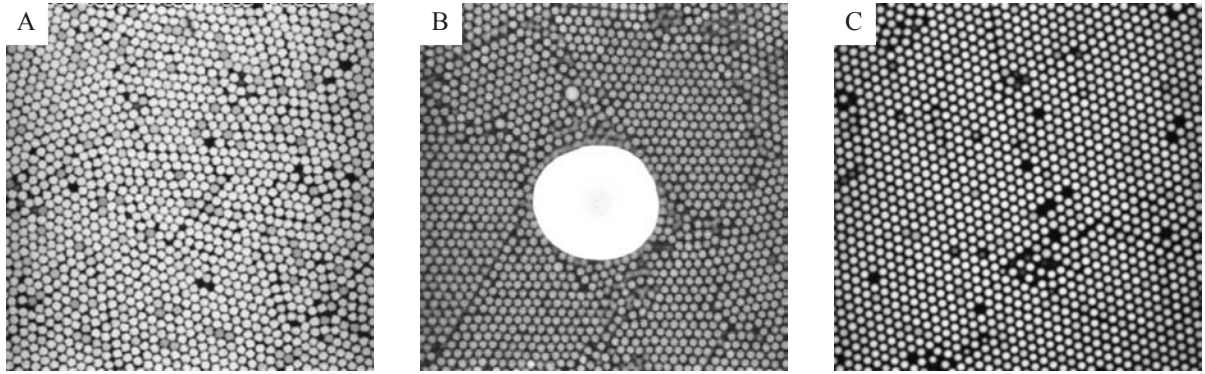


**Fig. 2.** Representative confocal images of (A) the polyhedrals ( $75 \times 75 \mu\text{m}^2$ ) and (B) the impurity system for  $\alpha = 13$  ( $60 \times 60 \mu\text{m}^2$ ) and (C) the reference spheres for the polyhedrals ( $75 \times 75 \mu\text{m}^2$ ). The system without impurities is equivalent to the image shown in (C).

The indices  $i$  and  $j$  run over all particles. The radial distribution functions for the polyhedral, the impurity and the reference systems are shown in Fig. 3 A1) and B1). We observe for the polyhedrals that the peaks in the  $g(r)$  are markedly broadened and that the structure in the  $g(r)$  decays much faster with respect to the reference  $g(r)$ . Nevertheless, the clear differences between the  $g(r)$  of the polyhedrals and the reference  $g(r)$  are not due to polycrystallinity. The polyhedral particle-shape frustrates the hexagonal crystal on the single-particle level, leading to significant differences between the radial distribution functions [37]. Moreover, the differences in the radial distribution functions observed in Fig. 3 A1), are similar to those observed in single-crystalline regions [37]. Thus, the  $g(r)$  is relatively insensitive to the presence of grain boundaries. This is corroborated by the impurity- $g(r)$ , which appears to be rather similar to that of the reference system without impurities. Hence, in the impurity system the crystals are not frustrated on the particle level, leading to similar radial distribution functions for the impurity and reference system despite the presence of grain boundaries. Note that the difference between the reference radial distribution functions in Fig. 3 A1) and B1) is due to a difference in volume fraction. Recall that the polyhedral system has been analyzed after sedimentation had fully completed, in contrast to the impurity system. The volume fraction can be quantified in terms of the two-dimensional packing fractions ( $\eta = N_T A_p / L^2$ , with  $N_T$  the total number of particles in the image and  $L^2$  the area of the image). Indeed, the more pronounced peaks in the reference  $g(r)$  in Fig. 3 A1) (polyhedrals) correspond to a packing fraction of  $\eta = 0.85$ , which is clearly higher than  $\eta = 0.74$  for the reference  $g(r)$  in Fig. 3 B1) (impurity system).

The loss of positional order shows up strongly in reciprocal space. The 2D structure factor is computed on a 2D grid of  $\mathbf{q}$ -values with a sampling rate of  $\pi/L$  with  $L$  the size of the microscopic image, as in [?]:

$$S_{\mathbf{q}} = \frac{1}{N} \left| \sum_{n=1}^N \exp(i(\mathbf{q} \cdot \mathbf{r}_n)) \right| \quad (2)$$

with  $\mathbf{r}_n$  the particle coordinates and  $N$  the total number of particles. The structure factor profile  $S(q)$  and the  $g(r)$  profile are two related but distinctly different representations. As will be shown in more detail below, the  $S(q)$  is more convenient for quantitative characterization of various types of long-range positional disorder, which is hidden in the details of the decay of the higher-order peaks of  $g(r)$ . The distinction between the finite-size effects (abrupt loss of the positional order) and the second-type disorder (monotonic deformation of the lattice) is extremely difficult on the basis of  $g(r)$  but is easily obtainable from  $S(q)$ . The structure factors are presented in figure 4 A) and B) for, respectively, the polyhedrals and the reference spheres. Whereas the spheres are monocrystalline, the  $S(q)$  for the polyhedrals is powderlike, with characteristic rings instead of sharp spots. A similar trend is observed for the impurity system and its reference system in figure 4 D) and E). A notable difference between the impurity system and the polyhedral system shows up in the radially averaged profiles, shown for the polyhedral system and the impurity system and their reference systems in figure 4 C) and figure 4 F) respectively. As was clear from the  $g(r)$  as well the positional order decays much faster in the polyhedral system. However, the angular profiles of the polyhedral system seem much wider than in the impurity system as well, which also follows from figure 4 A), where the intensity range used to depict the profile is much smaller than in figure 4 B). This seems to point to orientational changes within the grain for the polyhedral system.

The bond-orientational correlation function  $g_6(r)$  is significantly affected by the polycrystallinity, as is evident from Fig. 3 A2) and B2). The bond-orientational correlation function  $g_6(r)$  [47, 49] is defined as

$$g_6(r) = \langle \psi_6^*(0) \psi_6(r) \rangle \quad (3)$$

with

$$\psi_6(r_i) = \frac{1}{N} \sum_{j=1}^N \exp[6i\theta(r_{ij})]. \quad (4)$$

Here,  $\psi_6$  is the local bond-orientational order parameter, where the summation  $j$  runs over all, in total  $N$ , near-

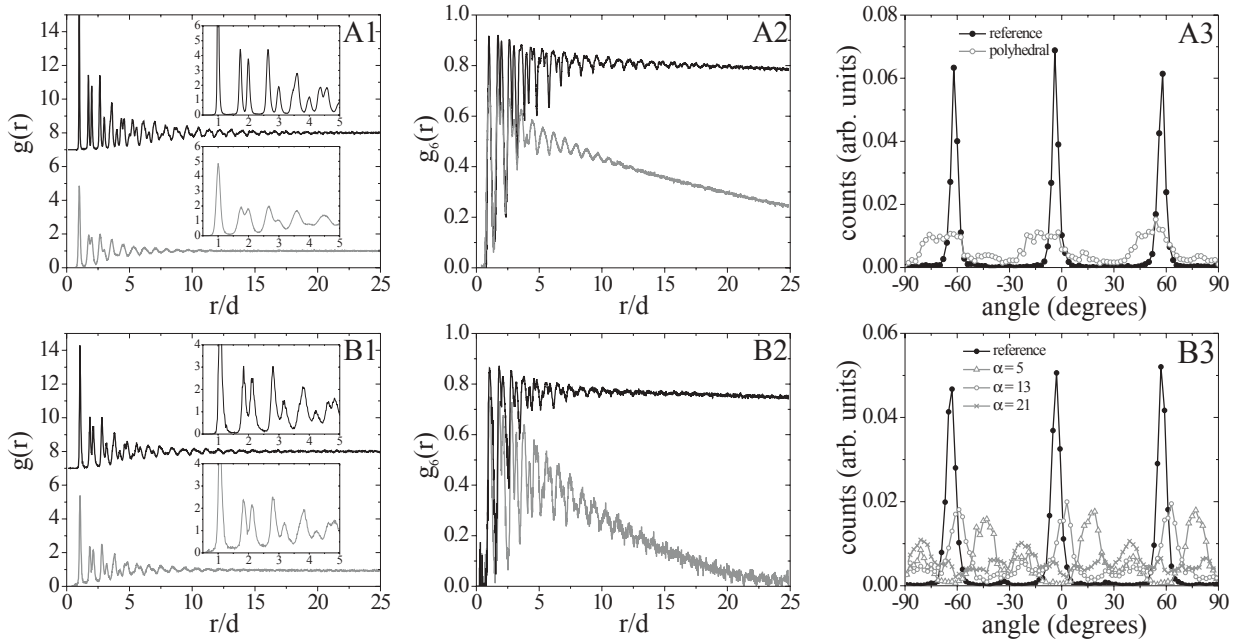


**Fig. 3.** (A1) Radial distribution functions  $g(r)$ , (A2) bond-orientational correlation functions  $g_6(r)$  and angle distributions (A3) for the polyhedrals (grey) and the reference spheres (black). (B1-B3) Same as A1-A3, but now for the impurity system (grey) and the reference system without impurities (black). (B1) and (B2):  $\alpha = 21$ , (B3):  $\alpha = 5, 13, 21$ . The radial distribution functions corresponding to the reference system have been vertically shifted for clarity. The insets in (A1 and B1) show an enlargement of the first peaks of  $g(r)$  to emphasize the differences between the geometrically frustrated and reference systems.

est neighbors of particle  $i$ .  $\theta(r_{ij})$  is the angle between the bond-vector connecting particles  $i$  and  $j$  and an arbitrary fixed reference axis. The  $\langle \rangle$  in Eq. (3) denote averaging over all pairs of particles and the index  $i$  in Eq. (4) runs over all particles. For both the polyhedral and the impurity system, the  $g_6(r)$  decays much faster than for the reference systems, indicating that the bond-orientational correlation is gradually lost in the frustrated systems. Indeed, polycrystallinity, where every crystallite has a different orientation, is expected to destroy the bond-orientational order on a length scale comparable to the grain size. Therefore, we determined the orientational correlation length  $\xi_O$  by fitting an exponentially decaying function to the envelope of  $g_6(r)$ : envelope of  $g_6(r) \propto \exp[-r/\xi_O]$  [47, 49, 51]. Hence,  $\xi_O$  is a measure for the typical size of the single crystalline domains. The orientational correlation length  $\xi_O$  being approximately 18 diameters for the polyhedrals and 9 diameters for the impurity system, indeed roughly corresponds to the grain size as can be inferred from the confocal images (Fig. 2A and B). Interestingly, no systematic trend in the grain size as a function of the size ratio  $\alpha$  was found, which suggests that the impurities act as immobile obstacles during the annealing of the grain boundaries. The bond-orientational correlation function of the reference systems show much slower, algebraic decay. The accompanying orientational correlation length  $\xi_O$  is more than 100 particle diameters for the reference systems, which points to the presence of long-range orientational order, i.e. large single-crystalline domains. Again,

the (minimal) difference between the  $g_6(r)$  of both reference systems can be attributed to the slightly different packing fraction.

Direct information about the polycrystallinity of a crystal structure is also given by orientational profile of the structure factor [51]. In Fig. 3A3) and B3), we show the real-space analog of this profile, that is, the distribution of angles that all nearest neighbor particles makes (with respect to an arbitrary reference axis). Clearly, in both reference systems three peaks at multiples of  $60^\circ$  are observed, corresponding to the three lattice orientations of a hexagonal crystal. Note that peaks with an orientational difference of  $180^\circ$  correspond to the same lattice orientation and are omitted for clarity. The absence of side-peaks points towards the single-crystalline structure of the reference colloidal crystals. The situation changes dramatically in the frustrated systems, where the peaks of the angle distributions are considerably broadened. Moreover, the angle distributions of the frustrated systems do not reach the zero baseline and show many other peaks. This is a direct consequence of the polycrystalline nature of the frustrated systems, as the presence of differently oriented crystalline domains results in broadening and eventually in a whole range of peaks in the angle distribution. We did not find a correlation between the orientations of the crystallites and the local curvature of the impurity, which is consistent with the absence of a relation between the grain size and the size ratio  $\alpha$ . Note that the peaks in the angle distribution of the impurity system are generally sharper than



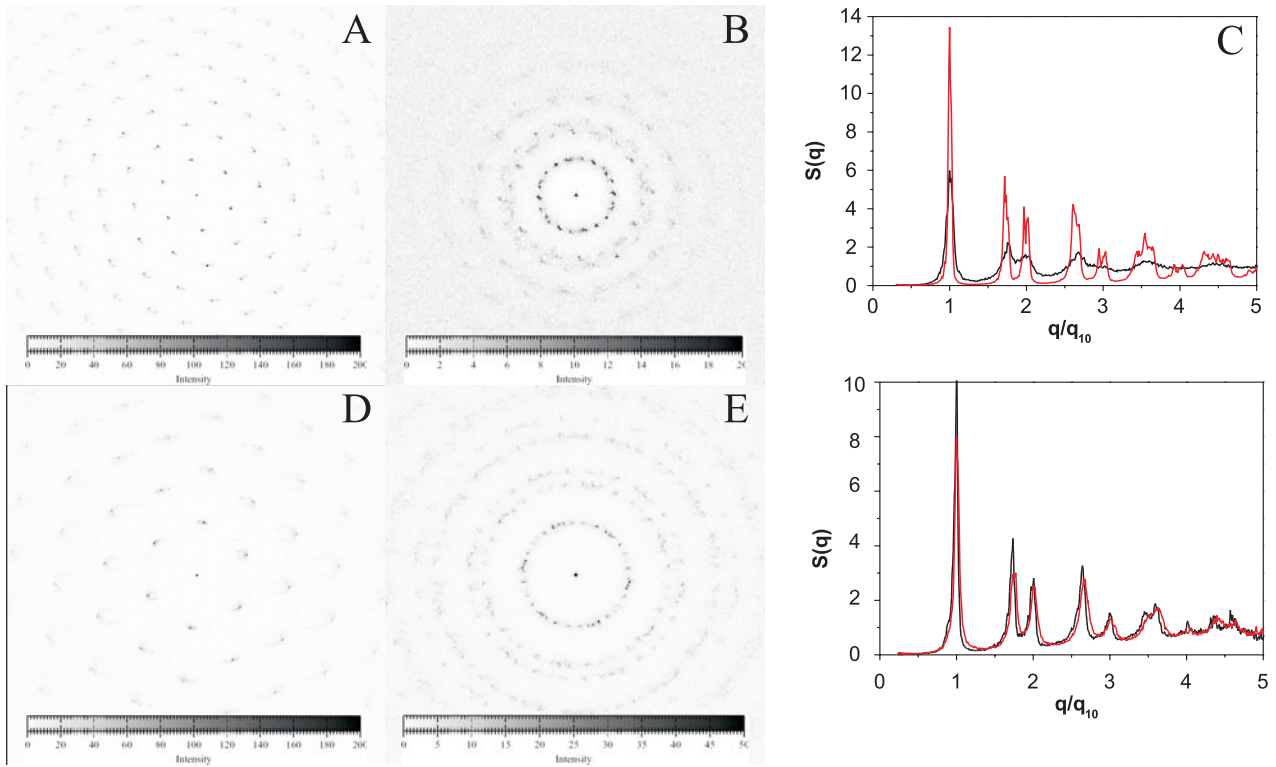


**Fig. 4.** The structure factor  $S(\mathbf{q})$  for the polyhedrals (A) and the impurity system (D). The reference structure factors for both systems are shown in panels B) and E). The radially averaged profiles are shown in panels C) and F). The structure factor for the potatoe system decays remarkably more rapidly.

those of the polyhedral system, which is related to the different nature of geometrical frustration in both systems: the orientation within the single grains is quite uniform in the impurity system, but changes much faster for the impurity system. This is illustrated in figure 5, which show plots of the particle positions with colors assigned based on the local  $\psi_6$  orientation. Within the grains, the orientation of the polyhedral sometimes changes within several color ranges, which is certainly not the case in the impurity and reference systems.

To elucidate how the grain boundaries are formed we studied the crystallization as a function of time. In Fig. 6 Delaunay triangulations corresponding to different stages during crystallization are presented. The color in the triangulations corresponds to the coordination number of the particles (see caption Fig. 6). In both the polyhedral and the impurity system, crystalline regions appear (Fig. 6A1, B1) simultaneously in different regions of the sample. These crystallites subsequently grow (Fig. 6A2-A4, B2-B4) and meet at a certain time. Due to the random orientations of the crystallites, grain boundaries are initially formed. This rules out the scenario that a single crystallite breaks into different crystallites due to the geometrical frustration. Interestingly, the reference systems crystallize similarly as the frustrated systems, resulting in a crystal that is initially relatively rich in grain boundaries [28,46]. However, the striking difference is that in the reference systems, the grain boundaries gradually anneal in time as is evident from Fig. 2C, whereas they persist in the

polyhedral and impurity system on our experimental time scales (Fig. 2A and B) [28]. In other words, the time scale associated with the reorientation of the different crystallites –necessary to form a single crystal– is much larger for the frustrated systems than for the reference systems.

The final structure in both systems studied here is determined by a subtle interplay between geometrical frustration, crystallization and kinetic arrest. Could it be that in the geometrically frustrated crystals the grain boundaries provide a route to minimize the stress in a similar way as the grain boundary scars that appear in a hexagonal crystal on a curved surface [25,26]? Despite their incommensurate shape, the polyhedral particles form hexagonal structures, with well defined and on average straight crystal axes [37]. Therefore, there it is unlikely that the introduction of a grain boundary reduces the stress in the crystal. However, due to the increased excluded volume with respect to a sphere, a polyhedral shape decreases the mobility of the particles, especially at high densities. As particle mobility drives the reorientation of crystallites, we argue that decreased mobility of the polyhedral particles leads to structural arrest of the crystallites, i.e. a “glass” of small, structurally arrested crystallites. The observation of vacancies and line defects (Fig. 2), which form due to the annealing of small crystallites, corroborate that the crystallization process has indeed been arrested. A similar argument can be given for the impurity system. An impurity locally introduces defects, but does not necessarily induce grain boundaries. Note that, if there exists

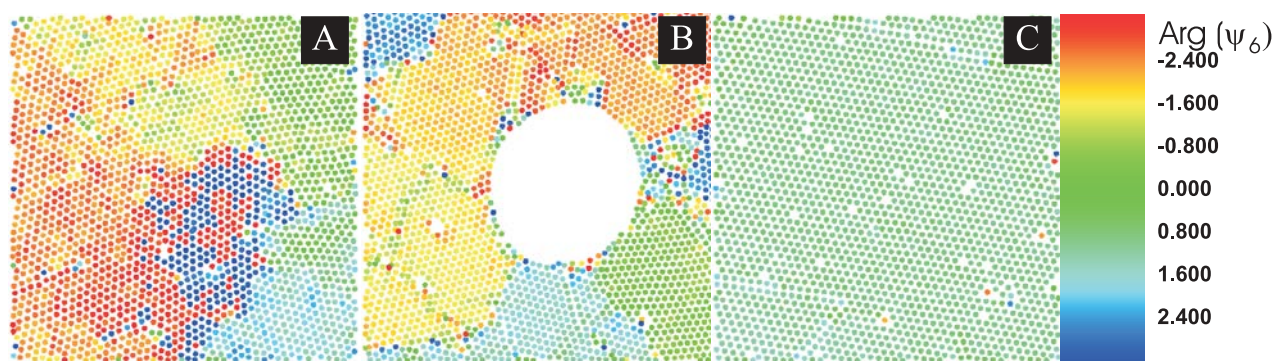


**Fig. 5.** (Color Online) Plots of (A) the polyhedral system, (B) the impurity system and (C) the polyhedral system. Particles are assigned a color based on their  $\psi_6$  orientation, as indicated in the legend of panel C). Within the grains, the reference system and the impurity system have a fairly uniform orientation, whereas the distribution of orientations within the polyhedral orientations is relatively broad.

a grain boundary, it is energetically favourable to annihilate some defects by locating the impurity in the grain boundary [15, 17, 51, 52]. Nevertheless, the impurities serve as immobile obstacles, which significantly slow down the reorientation-process of the crystallites around the impurity. Consequently, this structural arrest again leads to the formation of a polycrystalline glass around the impurities.

## 4 Conclusions

Colloidal systems provide a powerful, many-particle, experimental system that can provide valuable contributions to increase the understanding of the microscopic origins behind macroscopic properties of nanocrystalline materials and a valuable addition to the widely used computer simulation studies. In this work, we have shown how colloidal crystals can be used to demonstrate that two completely different ways of geometrical frustration both significantly decrease the grain size in materials: (I) frustration due to a polyhedral particle shape stabilizes small crystal grains on a single particle level whereas (II) frustration by the introduction of impurities stabilizes small crystallites on the single grain level. We expect that by increasing the roughness of the particle-shape or the concentration of the impurities, this structural arrest becomes more pronounced, which could be used to tune the grain size, to stabilize nanocrystalline materials and addressing fundamental issues in materials science [15–17, 53, 54]. Examples include designing highly ductile nanocrystalline materials [15–17, 53–55], tackling the microscopic origin of embrittlement due to impurities [14, 39] and understanding the high diffusivities and catalytic properties [56].

## 5 Acknowledgements

Hans Scherff and Esther Groeneveld are acknowledged for particle synthesis. This work is part of the research programme of the Stichting voor Fundamenteel Onderzoek der Materie (FOM), financially supported by the

Nederlandse Organisatie voor Wetenschappelijk Onderzoek (NWO). RPAD acknowledges the Alexander von Humboldt Foundation for financial support. Support through the Transregion Sonderforschungsbereich 6 (SFB TR6) through the Deutsche Forschungsgemeinschaft (DFG) is acknowledged.

## References

1. R. Phillips, *Crystals, defects and microstructure* (Cambridge University Press, Cambridge, 2001)
2. J.P. Hirth, J. Lothe, *Theory of dislocations*, 2nd edn. (Wiley, New York, 1982)
3. S.E. Offermans, N.H. van Dijk, J. Sietsma, S. Grigull, E.M. Lauridsen, L. Margulies, H.F. Poulsen, M.T. Rekveldt, S. van der Zwaag, *Science* **298**, 1003 (2002)
4. S. Yip, *Nature* **391**, 532 (1998)
5. J. Schiotz, F.D. Di Tolla, K.W. Jacobsen, *Nature* **391**, 561 (1998)
6. H. Van Swygenhoven, *Science* **296**, 66 (2002)
7. E.O. Hall, *Proc. Phys. Soc. Lond. B* **64**, 747 (1951)
8. N.J. Petch, *J. Iron Steel Inst.* **174**, 25 (1953)
9. H. Gleiter, *Acta Mater.* **48**, 1 (2000)
10. Q.H. Wei, X.L. Wu, *Phys. Rev. E* **70**, 020401(R) (2004)
11. H. Van Swygenhoven, D. Farkas, A. Caro, *Phys. Rev. B* **62**, 831 (2000)
12. P.M. Derlet, H. Van Swygenhoven, *Phys. Rev. B* **67**, 014202 (2003)
13. D. Wolf, V. Yamakov, S.R. Phillpot, A. Mukherjee, H. Gleiter, *Acta Mater.* **53**, 1 (2005)
14. R. Schweinfest, A.T. Paxton, M.W. Finnis, *Nature* **432**, 1008 (2004)
15. P.C. Millett, R.P. Selvam, S. Bansal, A. Saxena, *Acta Mater.* **53**, 3671 (2005)
16. P.C. Millett, R.P. Selvam, A. Saxena, *Acta Mater.* **54**, 297 (2006)
17. P.C. Millett, R.P. Selvam, A. Saxena, *Acta Mater.* **55**, 2329 (2007)
18. A. van Blaaderen, P. Wiltzius, *Science* **270**, 1177 (1995)
19. W.K. Kegel, A. van Blaaderen, *Science* **287**, 290 (2000)
20. E.R. Weeks, J.C. Crocker, A.C. Levitt, A. Schofield, D.A. Weitz, *Science* **287**, 627 (2000)



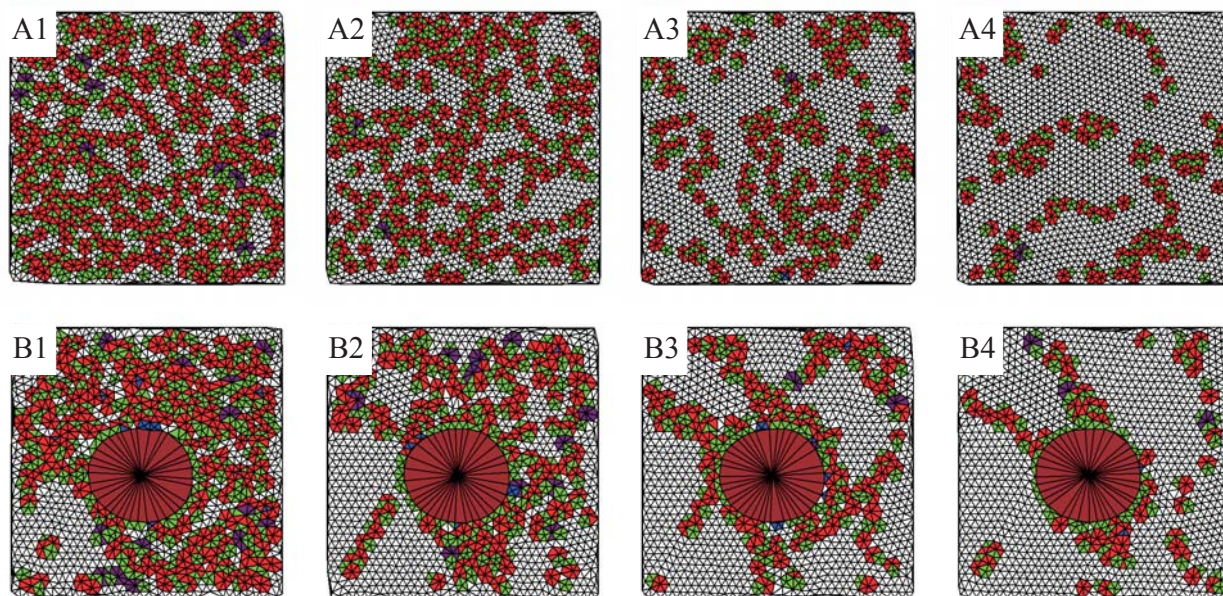


**Fig. 6.** (Color online) (A1-A4) Delaunay triangulations corresponding to different stages during crystallization of the polyhedral colloids ( $100 \times 100 \mu\text{m}^2$ ): A1-A4 respectively correspond to 0, 6, 12, 25 minutes after homogenization. (B1-B4) The same, but now for the impurity system with  $\alpha = 13$  ( $60 \times 60 \mu\text{m}^2$ ): B1-B4 respectively correspond to 41, 60, 65, 80 minutes after homogenization. The color code for the coordination number of the particles is as follows: four-fold: blue, five-fold: green, six-fold: red, seven-fold: purple and eight-fold: brown. The triangulation within the impurity has no physical meaning.

21. A. Pertsinidis, X.S. Ling, *Nature* **413**, 147 (2001)
22. S. Kodambaka, S.V. Khare, I. W. Swich, K. Ohmori, I. Petrov, J.E. Greene, *Nature* **429**, 49 (2004)
23. P. Schall, I. Cohen, D.A. Weitz, F. Spaepen, *Science* **305**, 1944 (2004)
24. R.P.A. Dullens, W.K. Kegel, *Phys. Rev. Lett.* **92**, 195702 (2004)
25. P. Lipowsky, M.J. Bowick, J.H. Meinke, D.R. Nelson, A.R. Bausch, *Nature Mater.* **4**, 407 (2005)
26. T. Einert, P. Lipowsky, J. Schilling, M.J. Bowick, A.R. Bausch, *Langmuir* **21**, 12076 (2005)
27. A. Pertsinidis, X.S. Ling, *New J. Phys.* **7**, 33 (2005)
28. V.W.A. Villeneuve, R.P.A. Dullens, D.G.A.L. Aarts, E. Groeneveld, J.H. Scherff, W.K. Kegel, H.N.W. Lekkerkerker, *Science* **309**, 1231 (2005)
29. A.M. Alsayed, M.F. Islam, J. Zhang, P.J. Collings, A.G. Yodh, *Science* **309**, 1207 (2005)
30. V.W.A. Villeneuve, D. Verboekend, R.P.A. Dullens, D.G.A.L. Aarts, W.K. Kegel, H.N.W. Lekkerkerker, *J. Phys.: Condens. Matter* **17**, S3371 (2005)
31. P. Schall, I. Cohen, D.A. Weitz, F. Spaepen, *Nature* **440**, 319 (2006)
32. R.P.A. Dullens, D.G.A.L. Aarts, W.K. Kegel, *Phys. Rev. Lett.* **97**, 228307 (2006)
33. A. Vrij, E.A. Nieuwenhuis, H.M. Fijnaut, W.G.M. Agterhof, *Faraday Discuss. Chem. Soc.* **65**, 101 (1978)
34. P.N. Pusey, W. van Megen, *Nature* **320**, 340 (1986)
35. P.N. Pusey, in *Liquids, Freezing and the Glass Transition*, edited by J.P. Hansen, D. Levesque, J. Zinn-Justin (Elsevier, Amsterdam, 1991)
36. W. van Megen, S. Underwood, *Nature* **362**, 616 (1993)
37. R.P.A. Dullens, M.C.D. Mourad, D.G.A.L. Aarts, J.P. Hoogenboom, W.K. Kegel, *Phys. Rev. Lett.* **96**, 028304 (2006)
38. R.W. Rice, *Ceramic Fabrication Technology* (Marcel Dekker, New York, 2003)
39. G. Duscher, M.F. Chisholm, U. Alber, M. Rühle, *Nature Mater.* **3**, 621 (2004)
40. R.H. Webb, *Rep. Prog. Phys.* **59**, 427 (1996)
41. R.P.A. Dullens, E.M. Claesson, W.K. Kegel, *Langmuir* **20**, 658 (2004)
42. G. Bosma, C. Pathmamanoharan, E.H.A. de Hoog, W.K. Kegel, A. van Blaaderen, H.N.W. Lekkerkerker, *J. Colloid Interface Sci.* **245**, 292 (2002)
43. E.H.A. de Hoog, W.K. Kegel, A. van Blaaderen, H.N.W. Lekkerkerker, *Phys. Rev. E* **64**, 021407 (2001)
44. R.P.A. Dullens, D.G.A.L. Aarts, W.K. Kegel, *Proc. Natl. Ac. Sci. USA* **103**, 529 (2006)
45. W. Schaertl, H. Sillescu, *J. Stat. Phys.* **77**, 1007 (1994)
46. J.P. Hoogenboom, P. Vergeer, A. van Blaaderen, *J. Chem. Phys.* **119**(6), 3371 (2003)
47. C.A. Murray, in *Bond-orientational order in condensed matter systems*, edited by K. Strandburg (Springer-Verlag, New York, 1992), pp. 137–215
48. J.C. Crocker, D.G. Grier, *J. Colloid Interface Sci.* **179**, 298 (1996)
49. D.R. Nelson, *Defects and geometry in condensed matter physics* (Cambridge University Press, Cambridge, 2002)
50. R.P.A. Dullens, A.V. Petukhov, *Europhys. Lett.* **77**, 58003 (2007)
51. D.R. Nelson, M. Rubinstein, *Philosophical Magazine A* **46**(1), 105 (1982)
52. Y. Ishida, S. Okamoto, S. Hachisu, *Acta Met.* **26**, 651 (1978)

- 53. J. Weissmüller, Nanostruct. Mater. **3**, 261 (1993)
- 54. C.E. Krill, R. Klein, S. Janes, R. Birringer, Mater. Sci. Forum **179 - 181**, 443 (1995)
- 55. J. Weissmüller, J. Markmann, Adv. Eng. Mat. **7**, 202 (2005)
- 56. C. Suryanarayana, Adv. Eng. Mat. **7**, 983 (2005)